International Journal of Solids and Structures 51 (2014) 2084–2095

Contents lists available at ScienceDirect

International Journal of Solids and Structures

journal homepage: www.elsevier.com/locate/ijsolstr

Some basic contact problems in couple stress elasticity

Th. Zisis [a], P.A. Gourgiotis [b,*], K.P. Baxevanakis [c], H.G. Georgiadis [c]

[a] Department of Civil Engineering, University of Thessaly, Volos GR-38336, Greece
[b] Department of Mechanical and Structural Engineering, University of Trento, Trento I-38123, Italy
[c] Mechanics Division, National Technical University of Athens, Zographou GR-15773, Greece

ARTICLE INFO

Article history:
Received 22 November 2013
Received in revised form 28 January 2014
Available online 25 February 2014

Keywords:
Contact
Indentation
Microstructure
Micromechanics
Couple-stress elasticity
Singular integral equations

ABSTRACT

Indentation tests have long been a standard method for material characterization due to the fact that they provide an easy, inexpensive, non-destructive and objective method of evaluating basic properties from small volumes of materials. As the contact scales in such experiments reduce progressively (micro to nano-scales) the internal material lengths become important and their effect upon the macroscopic response cannot be ignored. In the present study, we derive general solutions for three basic two-dimensional (2D) plane-strain contact problems within the framework of the generalized continuum theory of couple-stress elasticity. This theory introduces characteristic material lengths in order to describe the pertinent scale effects that emerge from the underlying microstructure and has proved to be very effective for modeling microstructured materials. By using this theory, we initially study the problem of the indentation of a deformable elastic half-plane by a flat punch, then by a cylindrical indentor, and finally by a shallow wedge indentor. Our approach is based on singular integral equations which have resulted from a treatment of the mixed boundary value problems via integral transforms and generalized functions. The results show significant departure from the predictions of classical elasticity revealing that it is inadequate to analyze indentation problems in microstructured materials employing only classical contact mechanics.

1. Introduction

Indentation tests have long been a standard method for material characterization due to the fact that they provide an easy, inexpensive, non-destructive and objective method of evaluating basic properties from small volumes of materials and thin films. A range of three-dimensional head-shapes are used including the sphere (Brinell test), the circular cone (Rockwell C), the three-sided pyramid (Berkovich) and the four-sided pyramid (Vickers), as well as a range of essentially two-dimensional indentors such as the wedge and the cylindrical (Fischer-Cripps, 2004; Johnson, 1985).

Studies have shown that there is a strong size effect on hardness in polycrystalline, cellular and polymer materials especially when the indent size is in the sub-micrometer depth regime. For example, the measured indentation hardness of metals and ceramics increases by a factor of two as the width of the indent is decreased from 10 to 1 μm (Ma and Clarke, 1995; Poole et al., 1996; Stelmashenko et al., 1993). In addition, indentation of thin films showed an increase in the yield stress with decreasing film thickness (Huber et al., 2002). Fleck et al. (1994) suggested that the size effect on hardness is related to the high stress/strain gradients present in shallow indentations. This dependence on stress/strain gradients can also be concluded from dislocation theory (Fleck et al., 1994). Moreover, Ma and Clarke (1995) observed that the variation of hardness with indentation size is consistent with a strain gradient plasticity model. In general, hardening of materials is due to the combined presence of geometrically necessary dislocations associated with plastic strain gradients and statistically stored dislocations associated with plastic strains. However, although strain gradients are extensively used to interpret the size effects in plastic deformation, they are also important for materials that deform elastically when the representative length of the deformation field becomes comparable to the lengths of the material microstructure. In fact, Maranganti and Sharma (2007) showed that gradient effects play a significant role in complex materials with coarse-grain structure. Indeed, Chen et al. (1998) developed a continuum model for cellular materials and concluded that the continuum description of these materials obeys a gradient elasticity theory of the couple-stress type. In the latter study, the intrinsic material length was naturally identified with the cell size. Moreover, gradient theories were successfully utilized in the past to

* Corresponding author. Tel.: +39 0461 282594; fax: +39 0461 282599.
E-mail address: p.gourgiotis@unitn.it (P.A. Gourgiotis).

http://dx.doi.org/10.1016/j.ijsolstr.2014.02.016
0020-7683/

model materials with microstructure like foams (Lakes, 1983) and porous solids (Lakes, 1993). Fleck and Shu (1995) showed the significance of strain gradient effects in the buckling of elastic fibers in composite materials. Size effects were also observed experimentally in post-buckling behavior of thin films (Fang and Wickert, 1994).

On the other hand, in indentation experiments at very small indentation depths, plastic flow does not occur until the equivalent strain reaches a critical yield value. In addition, the displacement recovered during unloading is largely elastic and for this reason the elastic contact theory is generally used in order to determine the elastic modulus from a simple analysis of the indentation load–displacement data (Pharr et al., 1992). Under these circumstances, the observed response of the material may be interpreted only through elasticity considerations. However, the classical elasticity theory includes no internal length scales and therefore is unable to predict the experimentally observed size effects. In fact, as the contact scales reduce progressively (micro to nano-scales) the internal material lengths become important and their effect upon the macroscopic response cannot be ignored. For this reason, generalized continuum theories, such as the micropolar theory, the couple stress theory, and the more general strain-gradient theory, may be employed to interpret the microstructure-dependent size effects on the elastic properties of the material. These theories capture the effects of microstructure by enriching the classical continuum with additional material characteristic length scales, and, thus, extending the range of applicability of the 'continuum' concept in an effort to bridge the gap between classical continuum theories and atomic-lattice theories. A recent review of generalized continuum theories can be found in Maugin (2010).

One of the most effective generalized continuum theories has proved to be that of couple-stress elasticity, also known as Cosserat theory with constrained rotations (Mindlin and Tiersten, 1962; Koiter, 1964). This theory is the simplest gradient theory in which couple-stresses make their appearance. The couple stress theory may be viewed as a generalization of classical elasticity theory and departs from the classical theory in several significant respects. In particular, the modified strain-energy density and the resulting constitutive relations involve besides the usual infinitesimal strains, certain strain gradients known as the rotation gradients. Also, the generalized stress–strain relations for the isotropic case include, in addition to the conventional pair of elastic constants, two new elastic constants, one of which is expressible in terms of a material parameter ℓ that has dimension of [length]. The presence of this length parameter, in turn, implies that the modified theory encompasses the analytical possibility of size effects, which are absent in the classical theory. A recent study by Bigoni and Drugan (2007) provides an interesting account of the determination of the couple-stress moduli via homogenization of heterogeneous materials. In addition, Beveridge et al. (2013) performed experiments and numerical simulations in heterogeneous materials loaded in bending and directly related the characteristic material lengths in couple-stress elasticity with the intrinsic geometrical structure of the samples. Experiments with phonon dispersion curves indicate that for most metals, the characteristic internal length is of the order of the lattice parameter, about 0.25 nm (Zhang and Sharma, 2005a). However, other small-molecule materials have larger internal characteristic lengths. For example, for the semiconductor gallium arsenide (GaAs), Zhang and Sharma (2005b) estimated a characteristic length of about 0.82 nm, while Reid and Gooding (1992) estimated a microstructural length for graphite of the order of 3.3 nm.

Couple-stress elasticity had already in the 60's and 70's some successful application on stress concentration problems concerning holes and inclusions. In recent years, there is a renewed interest in couple-stress theory dealing with problems of microstructured materials. This is due to the inability of the classical theory to predict experimental observed size effects and also due to the increased demands for manufacturing devices at very small scales. For instance, a multitude of problems concerning fracture, plasticity, dislocations, and wave propagation have been analyzed within the framework of couple stress and related gradient theories. Recent applications include work by, among others, Vardoulakis and Sulem (1995), Huang et al. (1999), Lubarda and Markenscoff (2000), Fleck and Hutchinson (2001), Georgiadis and Velgaki (2003), Grammenoudis and Tsakmakis (2005), Grentzelou and Georgiadis (2005), Radi (2007), Gourgiotis and Georgiadis (2008), Piccolroaz et al. (2012).

Regarding size effects in contact problems, we note that through the years various models have emerged in the literature to quantify the observed size effect in indentation. Most of these models are phenomenological in nature based on gradient plasticity ideas or on discrete dislocation concepts (see e.g. Poole et al., 1996; Begley and Hutchinson, 1998; Nix and Gao, 1998; Shu and Fleck, 1998; Wei and Hutchinson, 2003; Danas et al., 2012). Another approach in the context of classical plasticity theories considers the effect of several micromechanical lengths upon the macroscopic indentation response by directly incorporating the microstructural characteristics of the indented half-space through purely geometrical considerations (see e.g. Chen et al., 2004; Stupkiewicz, 2007; Fleck and Zisis, 2010; Zisis and Fleck, 2010).

On the other hand purely elastic indentation of materials is hard to achieve in practice (Larsson et al., 1996). Nonetheless, elasticity can be of interest in particular cases. In fact, there are materials such as polymers that exhibit significant size effects also in the elastic regime (Han and Nikolov, 2007; Nikolov et al., 2007). In general, as was pointed out by Maranganti and Sharma (2007), materials with explicit microstructure such as cellular materials, composites, ceramics, glassy and semi-crystalline polymers can be fruitfully modeled by using gradient type elasticity theories.

In the present paper, we deal with three basic plane-strain contact problems in couple-stress elasticity. It is remarked that Muki and Sternberg (1965) were the first to study the effects of couple-stresses upon the flat-punch indentation response employing the elaborate method of dual integral equations. In our work, we extend their study by considering different types of indentors and utilizing a more direct approach based on singular integral equations. It is worth noting that this is the first analytical approach in the literature examining the response of various types of indentors in 2D contact problems within the context of gradient type elasticity theories. The paper is organized as follows: Initially, we summarize the fundamental equations of couple-stress elasticity under plane-strain conditions. Then, we formulate the three plane-strain contact problems concerning the indentation of an elastic half-space by (i) a flat punch, (ii) a cylindrical indentor, and (iii) a wedge indentor. To obtain full field solutions the method of singular integral equations is utilized. More specifically, the integral equations have resulted from a treatment of the mixed boundary value problems via Fourier transforms and generalized functions. The integral equations are then solved by employing analytical and numerical considerations. In the final part, the results for the three different indentation methods are presented and the influence of microstructure upon the solution is discussed in detail.

We note that our analysis may have some genuine practical application in qualitatively identifying the influence of length scale effects in real materials and possibly even quantifying the length scale parameter itself. The requirement to identify such effects, at least qualitatively, by simple procedures is of real practical importance (Lakes et al., 1985).

2. Basic equations in plane-strain

We recall here briefly the main features of the equilibrium theory of plane strain within the linearized couple-stress theory of homogeneous and isotropic elastic solids. Detailed presentations of the couple-stress theory can be found in the fundamental papers of Mindlin and Tiersten (1962), and Koiter (1964). An interesting exposition of the theory under plane-strain conditions was given in the work by Muki and Sternberg (1965), and more recently by Gourgiotis and Georgiadis (2011).

For a body that occupies a domain in the (x,y)-plane under conditions of plane strain, the displacement field takes the general form:

$$u_x \equiv u_x(x,y) \neq 0,\ u_y \equiv u_y(x,y) \neq 0,\ u_z \equiv 0. \tag{1}$$

Further, for the kinematical description, the following quantities are defined in the framework of the geometrically linear theory

$$\varepsilon_{xx} = \frac{\partial u_x}{\partial x},\ \varepsilon_{yy} = \frac{\partial u_y}{\partial y},\ \varepsilon_{xy} = \varepsilon_{yx} = \frac{1}{2}\left(\frac{\partial u_y}{\partial x} + \frac{\partial u_x}{\partial y}\right), \tag{2}$$

$$\omega = \frac{1}{2}\left(\frac{\partial u_y}{\partial x} - \frac{\partial u_x}{\partial y}\right),\ \kappa_{xz} = \frac{\partial \omega}{\partial x},\ \kappa_{yz} = \frac{\partial \omega}{\partial y}, \tag{3}$$

where $\boldsymbol{\varepsilon}$ is the usual strain tensor, ω is the rotation, and $(\kappa_{xz}, \kappa_{yz})$ are the non-vanishing components of the curvature tensor (i.e. the gradient of rotation) expressed in dimensions of $[\text{length}]^{-1}$.

Accordingly, assuming vanishing body forces and body couples, the equations of equilibrium in the present circumstances reduce to

$$\frac{\partial \sigma_{xx}}{\partial x} + \frac{\partial \sigma_{yx}}{\partial y} = 0,\ \frac{\partial \sigma_{xy}}{\partial x} + \frac{\partial \sigma_{yy}}{\partial y} = 0,\ \sigma_{xy} - \sigma_{yx} + \frac{\partial m_{xz}}{\partial x} + \frac{\partial m_{yz}}{\partial y} = 0, \tag{4}$$

where $(\sigma_{xx}, \sigma_{yy}, \sigma_{yx}, \sigma_{xy})$ and $(m_{xz},\ m_{yz})$ are the non-vanishing components of the (asymmetric) stress and couple-stress tensors, respectively. Moreover, the constitutive equations furnish

$$\varepsilon_{xx} = (2\mu)^{-1}[\sigma_{xx} - \nu(\sigma_{xx} + \sigma_{yy})],$$
$$\varepsilon_{yy} = (2\mu)^{-1}[\sigma_{yy} - \nu(\sigma_{xx} + \sigma_{yy})],\ \varepsilon_{xy} = (4\mu)^{-1}(\sigma_{xy} + \sigma_{yx}), \tag{5}$$

and

$$\kappa_{xz} = (4\mu\ell^2)^{-1} m_{xz},\ \kappa_{yz} = (4\mu\ell^2)^{-1} m_{yz}. \tag{6}$$

where μ, ν and ℓ, in this order, stand for the shear modulus, Poisson's ratio, and the characteristic material length of couple-stress theory (Mindlin, 1963).

Combing the previous equations, we obtain the following stress and couple-stress equations of compatibility

$$\frac{\partial^2 \sigma_{xx}}{\partial y^2} - \frac{\partial^2}{\partial x \partial y}(\sigma_{xy} + \sigma_{yx}) + \frac{\partial^2 \sigma_{yy}}{\partial x^2} = \nu \nabla^2 (\sigma_{xx} + \sigma_{yy}), \tag{7}$$

$$\frac{\partial m_{xz}}{\partial y} = \frac{\partial m_{yz}}{\partial x}, \tag{8}$$

$$m_{xz} = -2\ell^2 \frac{\partial}{\partial y}[\sigma_{xx} - \nu(\sigma_{xx} + \sigma_{yy})] + \ell^2 \frac{\partial}{\partial x}(\sigma_{xy} + \sigma_{yx}), \tag{9}$$

$$m_{yz} = 2\ell^2 \frac{\partial}{\partial x}[\sigma_{yy} - \nu(\sigma_{xx} + \sigma_{yy})] - \ell^2 \frac{\partial}{\partial y}(\sigma_{xy} + \sigma_{yx}). \tag{10}$$

Note that only three of the four equations of compatibility are independent. Indeed, Eqs. (8)–(10) imply (7), while Eqs. (7), (9), and (10) yield (8) (Mindlin, 1963; Muki and Sternberg, 1965).

Finally, Mindlin (1963) introduced pertinent stress functions (generalizing the Airy stress function of classical elasticity) by showing that the complete solution of Eq. (4) admits the following representation

$$\sigma_{xx} = \frac{\partial^2 \Phi}{\partial y^2} - \frac{\partial^2 \Psi}{\partial x \partial y},\ \sigma_{yy} = \frac{\partial^2 \Phi}{\partial x^2} + \frac{\partial^2 \Psi}{\partial x \partial y},\ \sigma_{xy} = -\frac{\partial^2 \Phi}{\partial x \partial y} - \frac{\partial^2 \Psi}{\partial y^2},$$
$$\sigma_{yx} = -\frac{\partial^2 \Phi}{\partial x \partial y} + \frac{\partial^2 \Psi}{\partial x^2}, \tag{11}$$

and

$$m_{xz} = \frac{\partial \Psi}{\partial x},\ m_{yz} = \frac{\partial \Psi}{\partial y}, \tag{12}$$

where $\Phi \equiv \Phi(x,y)$ and $\Psi \equiv \Psi(x,y)$ are two arbitrary but sufficiently smooth functions. Further, substitution of (11) and (12) into (9) and (10) results in the following pair of differential equations for the stress functions

$$\frac{\partial}{\partial x}(\Psi - \ell^2 \nabla^2 \Psi) = -2(1-\nu)\ell^2 \nabla^2 \left(\frac{\partial \Phi}{\partial y}\right), \tag{13}$$

$$\frac{\partial}{\partial y}(\Psi - \ell^2 \nabla^2 \Psi) = 2(1-\nu)\ell^2 \nabla^2 \left(\frac{\partial \Phi}{\partial x}\right), \tag{14}$$

which then lead to the uncoupled PDEs

$$\nabla^4 \Phi = 0, \tag{15}$$

$$\nabla^2 \Psi - \ell^2 \nabla^4 \Psi = 0. \tag{16}$$

Note that as the quantities ℓ, $\partial\Psi/\partial$x and $\partial\Psi/\partial$y tend to zero, the above representation passes over into the classical Airy's representation. In addition, from (2), (3), (5) and (11), (12), one can obtain the following relations expressing the displacement field in terms of Mindlin's stress functions

$$\frac{\partial u_x}{\partial x} = \frac{1}{2\mu}\left(\frac{\partial^2 \Phi}{\partial y^2} - \frac{\partial^2 \Psi}{\partial x \partial y} - \nu \nabla^2 \Phi\right), \tag{17}$$

$$\frac{\partial u_y}{\partial y} = \frac{1}{2\mu}\left(\frac{\partial^2 \Phi}{\partial x^2} + \frac{\partial^2 \Psi}{\partial x \partial y} - \nu \nabla^2 \Phi\right), \tag{18}$$

$$\frac{\partial u_x}{\partial y} + \frac{\partial u_y}{\partial x} = -\frac{1}{2\mu}\left(2\frac{\partial^2 \Phi}{\partial x \partial y} - \frac{\partial^2 \Psi}{\partial x^2} + \frac{\partial^2 \Psi}{\partial y^2}\right). \tag{19}$$

3. Formulation of the contact problems and boundary conditions

We now examine the stresses produced in an elastic half-plane by the action of a rigid indentor pressed into the surface as shown in Fig. 1. The body is governed by the equations of couple-stress elasticity and a Cartesian coordinate system $Oxyz$ is attached at the center line of the indentor's geometry (Fig. 1). A load P is applied at the center line of the indentor which, in our plane strain case, has dimensions of $[\text{force}][\text{length}]^{-1}$.

Three basic indentor profiles are considered. Firstly, we study the flat punch indentation problem (Fig. 1a). We assume that the punch has a flat base of width $2b$ with sharp square corners; it is sufficiently long in the z-direction so that plane strain conditions prevail. Since the punch is rigid, the surface of the elastic solid remains flat in the contact area. In addition, we restrict our study to indentations in which the punch does not tilt, so that the interface remains parallel to the undeformed surface of the solid – the response upon tilting is examined in a subsequent paper. Next, we examine a rigid cylindrical indentor of radius R with its axis lying parallel to the z-axis and pressed in contact with a half-plane under the action of the force P. The two bodies are making contact over a

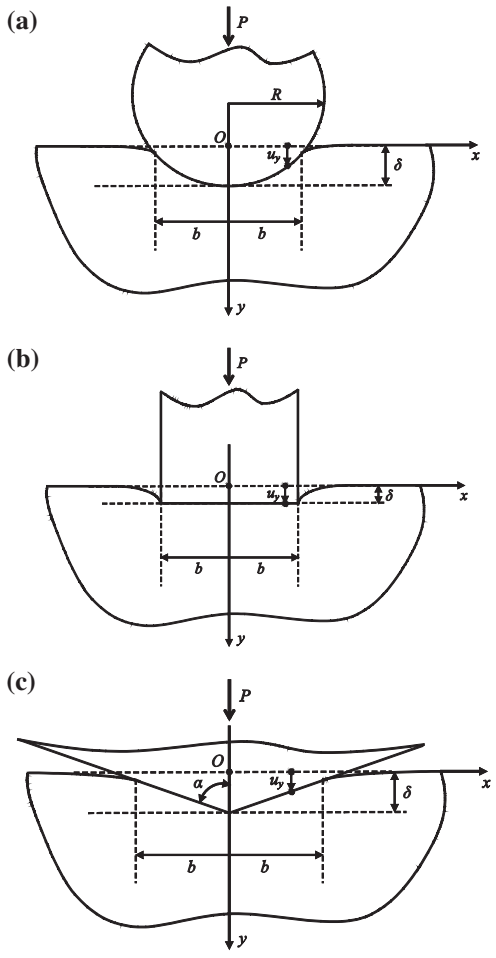

Fig. 1. Indentation of an elastic traction-free half-space by a rigid: (a) flat punch (b) cylindrical indentor (c) wedge indentor.

long strip of width $2b$ lying parallel to the z-axis (Fig. 1b). In classical elasticity Hertz considered this case as the limit of an elliptical contact when one axis of the ellipse becomes considerably larger than the other axis (see e.g. Hills and Nowell, 1994). Finally, we consider a shallow wedge indentor pressed in contact with a half-plane under the action of the force P. In order for the deformations to be sufficiently small, within the frame of the geometrically linear theory, the semi-angle α of the wedge must be close to 90° (in our case we assume that $\alpha = 88^\circ$; see also Johnson, 1985).

For the points lying within the contact area ($-b < x < b$) after loading, we have the following general geometrical boundary condition:

$$u_y = k(x), \tag{20}$$

which, depending on the type of the profile, takes three alternative forms:

(i) $k(x) = \delta$, for the case of the flat punch,
(ii) $k(x) = \delta - \frac{1}{2R}x^2$, for the case of the cylindrical indentor,
(iii) $k(x) = \delta - |x|\cot\alpha$, for the case of the wedge indentor.

where δ is a positive constant.

Regarding the traction boundary conditions of the contact problem, we note first that no restriction is imposed on the tangential displacement u_x and its normal derivative du_x/dy under the indentor. Consequently, the rotation ω is arbitrary at the contact area. Thus, by enforcing the principle of virtual power (Koiter, 1964), we may approximate zero shear and couple tractions under the indentor. In view of the above, the following traction boundary conditions hold for a frictionless and smooth contact (see also Shu and Fleck, 1998):

$$\sigma_{yy}(x,0) = 0 \quad \text{for } |x| > b, \tag{21}$$

$$\sigma_{yx}(x,0) = 0 \quad \text{for } -\infty < x < \infty, \tag{22}$$

$$m_{yz}(x,0) = 0 \quad \text{for } -\infty < x < \infty, \tag{23}$$

which are accompanied by the *complementary* condition

$$\int_{-b}^{b} \sigma_{yy}(x,0)dx = -\int_{-b}^{b} p(x)dx = -P, \tag{24}$$

where P is the applied line load, and $\sigma_{yy}(x,0) = -p(x)$ is the pressure below the indentor with the following properties:

$$p(x) = 0 \ (|x| > b) \quad \text{and} \quad p(x) = p(-x) \ (|x| < b). \tag{25}$$

Moreover, since the indented surface is an unbounded region, the above boundary conditions must be supplemented by the regularity conditions at infinity

$$\sigma_{ij} \to 0 \quad \text{as} \quad \rho \equiv \sqrt{x^2 + y^2} \to \infty. \tag{26}$$

As a final comment, before proceeding, we should note that in 2D contact problems a difficulty arises regarding the evaluation of the displacements, which is absent in the 3D cases. Indeed, as discussed in Johnson (1985), the value of the displacement of a point in an elastic half-space loaded two dimensionally cannot be expressed relative to a datum located at infinity, due to the fact that the displacements become unbounded as $O(\ln \rho)$, with ρ being the distance from the loaded zone. Thus, the normal displacement u_y can only be defined relative to an arbitrary chosen datum. In physical terms this means that the distance δ cannot be evaluated by consideration of the local contact stresses alone; it is also necessary to consider the stress distribution within the bulk of the body (see also Bower, 2009).

4. Fourier transform analysis

The three plane-strain contact problems are attacked with the aid of the Fourier transform on the basis of the stress function formulation summarized earlier. The direct Fourier transform and its inverse are defined as follows

$$\hat{f}(\xi) = \int_{-\infty}^{\infty} f(x) e^{i\xi x} dx, \tag{27}$$

$$f(x) = \frac{1}{2\pi} \int_{-\infty}^{\infty} \hat{f}(\xi) e^{-i\xi x} d\xi, \tag{28}$$

where $i \equiv (-1)^{1/2}$.

Transforming now (15) and (16) with (27) provides the following ODEs for the transformed stress functions

$$\frac{d^4\hat{\Phi}}{dy^4} - 2\xi^2 \frac{d^2\hat{\Phi}}{dy^2} + \xi^4 \hat{\Phi} = 0, \tag{29}$$

$$\ell^2 \frac{d^4\hat{\Psi}}{dy^4} - (1 + 2\ell^2\xi^2)\frac{d^2\hat{\Psi}}{dy^2} + \xi^2(1 + \ell^2\xi^2)\hat{\Psi} = 0. \tag{30}$$

Similarly, the following results are obtained for the Fourier transforms of the stresses, couple-stresses and displacements

$$\hat{\sigma}_{xx} = \frac{d^2\hat{\Phi}}{dy^2} + i\xi\frac{d\hat{\Psi}}{dy}, \ \hat{\sigma}_{yy} = -\xi^2\hat{\Phi} - i\xi\frac{d\hat{\Psi}}{dy}, \ \hat{\sigma}_{yx} = i\xi\frac{d\hat{\Phi}}{dy} - \xi^2\hat{\Psi},$$
$$\hat{\sigma}_{xy} = i\xi\frac{d\hat{\Phi}}{dy} - \frac{d^2\hat{\Psi}}{dy^2}, \tag{31}$$

$$\hat{m}_{xz} = -i\xi\hat{\Psi},\ \hat{m}_{yz} = \frac{d\hat{\Psi}}{dy}. \tag{32}$$

$$\begin{aligned}\hat{u}_x &= \frac{1}{2\mu\xi}\left(i(1-\nu)\frac{d^2\hat{\Phi}}{dy^2} - \xi\frac{d\hat{\Psi}}{dy} + i\nu\xi^2\hat{\Phi}\right),\\ \hat{u}_y &= \frac{1}{2\mu\xi^2}\left((1-\nu)\frac{d^3\hat{\Phi}}{dy^3} - (2-\nu)\xi^2\frac{d\hat{\Phi}}{dy} - i\xi^3\hat{\Psi}\right).\end{aligned} \tag{33}$$

The governing equations (29) and (30) have the following general solution that is required to be bounded as $y \to +\infty$

$$\hat{\Phi}(\xi, y) = [C_1(\xi) + yC_2(\xi)]e^{-|\xi|y}, \tag{34}$$

$$\hat{\Psi}(\xi, y) = C_3(\xi)e^{-|\xi|y} + C_4(\xi)e^{-\gamma y}, \tag{35}$$

where $\gamma \equiv \gamma(\xi) = (1/\ell^2 + \xi^2)^{1/2}$.

Enforcing now the boundary conditions (22) and (23) results in the following equations for the unknown functions $C_i(\xi)$ $(i = 1, \ldots, 4)$

$$C_2(\xi) = |\xi|C_1(\xi) - i\xi(1 - |\xi|^{-1}\gamma)C_4(\xi), \tag{36}$$

$$C_3(\xi) = -\gamma|\xi|^{-1}C_4(\xi), \tag{37}$$

where the functions $C_2(\xi)$ and $C_3(\xi)$ are related through the compatibility equations (13) and (14) as follows

$$C_3(\xi) = -4i\ell^2(1-\nu)\xi C_2(\xi). \tag{38}$$

Further, according to (21), (24), and (27), we obtain

$$\hat{\sigma}_{yy}(\xi, 0) = \int_{-\infty}^{\infty}\sigma_{yy}(x, 0)e^{i\xi x}dx = -\int_{-b}^{b}p(x)e^{i\xi x}dx = -\hat{p}(\xi), \tag{39}$$

where $\hat{p}(\xi)$ is the transformed pressure distribution below the indentor, which, taking into account the second of (31) can be written as

$$\hat{p}(\xi) = \xi^2\hat{\Phi} + i\xi\frac{d\hat{\Psi}}{dy}. \tag{40}$$

Moreover, upon substituting (34) and (35) into (40) for $y = 0$, and taking also into account (36)–(38), we obtain the relation

$$C_1(\xi) = \frac{\hat{p}(\xi)}{\xi^2}. \tag{41}$$

Finally, in view of (36)–(41), the transformed stress functions become now

$$\hat{\Phi}(\xi, y) = \left[1 + \frac{|\xi|\gamma y}{\gamma - 4(1-\nu)\ell^2\xi^2(|\xi| - \gamma)}\right]\frac{e^{-|\xi|y}}{\xi^2}\hat{p}(\xi), \tag{42}$$

$$\hat{\Psi}(\xi, y) = -\frac{4i\ell^2(1-\nu)[|\xi|\gamma e^{-\beta y} - \xi^2 e^{-\gamma y}]}{[\gamma - 4(1-\nu)\ell^2\xi^2(|\xi| - \gamma)]\xi}\hat{p}(\xi). \tag{43}$$

5. Singular integral equation approach

Our objective now is the determination of the contact-stress distribution $p(x)$ under the indentor and the determination of the pertinent contact length b when appropriate. For the solution of the mixed boundary value problems, we employ the method of singular integral equations. In classical elasticity, the general procedure of reducing mixed boundary value problems to singular integral equations is given, e.g. by Erdogan (1978). An application of the technique within the context of couple-stress elasticity for plane-strain crack problems can be found in Gourgiotis and Georgiadis (2007, 2008), and in the context of strain-gradient elasticity in Paulino et al. (2003) and Gourgiotis and Georgiadis (2009).

The definition of the inverse Fourier transform in (28) together with the second of (33), lead to the following equation

$$\begin{aligned}\frac{du_y}{dx} = &\frac{1}{2\pi}\\ &\times\int_{-\infty}^{\infty}\left(\frac{-i}{2\mu\xi}\left((1-\nu)\frac{d^3\hat{\Phi}}{dy^3} - (2-\nu)\xi^2\frac{d\hat{\Phi}}{dy} - i\xi^3\hat{\Psi}\right)\right)e^{-ix\xi}d\xi.\end{aligned} \tag{44}$$

By substituting in the above equation the expressions for the stress functions (42) and (43) at $y = 0$, and by taking into account (39), we obtain

$$\begin{aligned}\frac{du_y}{dx} = &\frac{1}{2\pi}\int_{-\infty}^{\infty}\frac{i(1-\nu)|\xi|\gamma}{\mu\xi[4\ell^2(1-\nu)\xi^2(|\xi| - \gamma) - \gamma]}\\ &\times\left[\int_{-b}^{b}p(s)e^{i\xi s}ds\right]e^{-ix\xi}d\xi.\end{aligned} \tag{45}$$

Then, using the displacement boundary condition in (20) and reversing the order of integration in (45), the problem is reduced to the following integral equation

$$\begin{aligned}&\frac{1}{2\pi}\int_{-b}^{b}p(s)\int_{-\infty}^{\infty}\left[\frac{i(1-\nu)|\xi|\gamma}{\mu\xi[4\ell^2(1-\nu)\xi^2(|\xi| - \gamma) - \gamma]}\right]e^{-i(x-s)\xi}d\xi ds\\ &= \frac{dk(x)}{dx},\ |x| \leqslant b,\end{aligned} \tag{46}$$

which, bearing in mind that the quantity inside the bracket is an odd function with respect to ξ, can be finally written as

$$\frac{1}{\mu\pi}\int_{-b}^{b}K(x-s)p(s)ds = \frac{dk(x)}{dx}, \tag{47}$$

where the kernel $K(x - s)$ is defined as

$$K(x-s) = \int_0^{\infty}g(\xi)\sin(\xi(x-s))d\xi, \tag{48}$$

with

$$g(\xi) = \frac{(1-\nu)\sqrt{1+\ell^2\xi^2}}{(4(1-\nu)\ell^3\xi^3 - 4(1-\nu)\ell^2\xi^2\sqrt{1+\ell^2\xi^2} - \sqrt{1+\ell^2\xi^2})}. \tag{49}$$

In Eq. (47), passing to the limit as $\ell \to 0$, one recovers the classical integral equation for each of the three characteristic 2D problems discussed in the present work.

Now, in order to make the kernel in (48) explicit and separate its singular and regular parts, it is necessary to examine the asymptotic behavior of the function $g(\xi)$ as $\xi \to \infty$. Indeed, by using theorems of the Abel-Tauber type (Roos, 1969) and noting that $\lim_{\xi\to\infty}g(\xi) = g_\infty(\xi) = -\frac{1-\nu}{3-2\nu}$, we decompose $g(\xi)$ as

$$g(\xi) = g_\infty(\xi) + [g(\xi) - g_\infty(\xi)]. \tag{50}$$

Accordingly, utilizing certain results of the theory of the generalized functions and singular distributions (Roos, 1969; Erdogan, 1978) the kernel $K(x - s)$ becomes

$$\begin{aligned}K(x-s) &= \underbrace{\int_0^{\infty}g_\infty(\xi)\sin(\xi(x-s))d\xi}_{\text{singular part}} + \underbrace{\int_0^{\infty}[g(\xi) - g_\infty(\xi)]\sin(\xi(x-s))d\xi}_{\text{regular part}}\\ &= -\frac{1-\nu}{(3-2\nu)}\frac{1}{x-s} + N(x-s),\end{aligned} \tag{51}$$

where

$$N(x-s)=\int_0^\infty [g(\xi)-g_\infty(\xi)]\sin(\xi(x-s))d\xi, \tag{52}$$

is now a regular kernel for $x\to s$.

In view of the above and after the appropriate normalization, the governing *singular* integral equation takes its final form

$$-\frac{1-\nu}{3-2\nu}\int_{-1}^{1}\frac{p(\tilde{s})}{\tilde{x}-\tilde{s}}d\tilde{s}+\int_{-1}^{1}\tilde{N}(\tilde{x}-\tilde{s})p(\tilde{s})d\tilde{s}=\frac{\mu\pi}{b}\frac{dk(\tilde{x})}{d\tilde{x}},\quad |\tilde{x}|<1, \tag{53}$$

with $\tilde{x}=x/b$, $\tilde{s}=s/b$. In addition, the complementary condition in (24) becomes

$$\int_{-1}^{1}p(\tilde{s})d\tilde{s}=Pb^{-1}. \tag{54}$$

It should be noted that the first integral in the integral equation (53) is interpreted in the Cauchy principal value sense (CPV). In addition, the regular kernel is defined as

$$\tilde{N}(\tilde{x}-\tilde{s})=\int_0^\infty\left[\frac{2(1-\nu)^2\left(2q^2\zeta^2\left(\sqrt{1+q^2\zeta^2}-q\zeta\right)-\sqrt{1+q^2\zeta^2}\right)}{(3-2\nu)\left(\sqrt{1+q^2\zeta^2}+4q^2(1-\nu)\zeta^2\left(\sqrt{1+q^2\zeta^2}-q\zeta\right)\right)}\right]\times\sin(\zeta(\tilde{x}-\tilde{s}))d\zeta, \tag{55}$$

with $\zeta=\xi b$ and $q=\ell/b$. The above convergent integral is a Fourier sine transform and can be efficiently evaluated numerically employing MATHEMATICA™ algorithms that take into account its oscillatory character.

6. Numerical solution

The numerical solution of the singular integral equation (53) is accomplished utilizing the collocation method with respect to each indentor profile.

6.1. Flat punch

The problem of the flat punch indenting a half-space in the context of couple-tress theory was initially treated by Muki and Sternberg (1965). The latter employed the elaborate method of dual integral equations. Based on their asymptotic analysis, we assume a pressure distribution of the form:

$$p(\tilde{s})=\sum_{n=0}^{\infty}a_n\frac{T_n(\tilde{s})}{\sqrt{1-\tilde{s}^2}},\quad |\tilde{s}|\leqslant 1, \tag{56}$$

where $T_n(\tilde{s})$ are the Chebyshev polynomials of the first kind (see e.g. Abramowitz and Stegun, 1972). We note that by assuming the above pressure representation, the classical square-root stress singularity at the corners of the punch is retained also in the couple stress theory. Now, substituting (56) into the integral equation (53) one arrives at

$$\sum_{n=0}^{\infty}a_n\left\{-\frac{1-\nu}{3-2\nu}\int_{-1}^{1}\frac{T_n(\tilde{s})}{\sqrt{1-\tilde{s}^2}(\tilde{x}-\tilde{s})}d\tilde{s}+\int_{-1}^{1}\frac{T_n(\tilde{s})}{\sqrt{1-\tilde{s}^2}}\tilde{N}(\tilde{x}-\tilde{s})d\tilde{s}\right\}=0,\quad |\tilde{x}|\leqslant 1. \tag{57}$$

Further, by using Eqs. (54), (56) and employing the orthogonality properties of the Chebyshev polynomials of the first kind, we derive that: $a_0=P(\pi b)^{-1}$, where $2b$ is the contact length which in the present case is constant. It is noted that the first integral in (57) is evaluated as a CPV integral by using the following properties of Chebyshev polynomials (Erdogan and Gupta, 1972)

$$\int_{-1}^{1}\frac{T_n(\tilde{s})}{\sqrt{1-\tilde{s}^2}(\tilde{x}-\tilde{s})}d\tilde{s}=\begin{cases}0 & \text{if } n=0\\ -\pi U_{n-1}(\tilde{x}), & \text{if } n\geqslant 1\end{cases},\quad |\tilde{x}|\leqslant 1, \tag{58}$$

where $U_n(\tilde{x})$ are Chebyshev polynomials of the second kind. The second integral in (57) is regular and can be readily obtained by the Gauss–Chebyshev quadrature method. Consequently, the singular integral equation (57) takes the following functional form

$$\sum_{n=0}^{\infty}a_n\left\{\frac{(1-\nu)\pi}{3-2\nu}U_{n-1}(\tilde{x})+Q_n(\tilde{x})\right\}=0,\quad |\tilde{x}|\leqslant 1, \tag{59}$$

with $Q_n(\tilde{x})=\int_{-1}^{1}T_n(\tilde{s})(1-\tilde{s}^2)^{-1/2}\tilde{N}(\tilde{x}-\tilde{s})d\tilde{s}$.

Now, Eq. (59) is solved by truncating the series at $n=N$ and using an appropriate collocation technique with collocation points chosen as the roots of $U_N(\tilde{x})$, viz. $\tilde{x}_j=\cos(j\pi/(N+1))$ with $j=1,2,\ldots,N$. In this way, a system of linear algebraic equations is formed which supplemented by the complementary condition (54) enables us to evaluate the $N+1$ coefficients a_n and, consequently, the desired pressure distribution. In Table 1, the convergence of the normalized pressure $p(\tilde{x})/p_{clas}(\tilde{x})$ below the indentor at the vicinity of the contact is presented. Note that for decreasing values of q, a larger number of collocation points is needed.

6.2. Cylindrical indentor

Next, we consider the problem of the cylindrical indentor. In classical elasticity the contact tractions are not singular at $x=\pm b$ (Johnson, 1985). Accordingly, guided by the results concerning the modification of stress singularities in the presence of couple stresses (Sternberg and Muki, 1967; Gourgiotis and Georgiadis, 2008), and also bearing in mind that the governing singular integral equation (53) has *qualitatively* the same general form with the respective one in the classical theory (with the addition of the regular kernel), we assume the following pressure distribution under the indentor

$$p(\tilde{s})=\sum_{n=0}^{\infty}a_nU_n(\tilde{s})\sqrt{1-\tilde{s}^2}. \tag{60}$$

In this case, the integral equation in (53) becomes

$$\sum_{n=0}^{\infty}a_n\left\{-\frac{1-\nu}{3-2\nu}\int_{-1}^{1}\frac{U_n(\tilde{s})\sqrt{1-\tilde{s}^2}}{(\tilde{x}-\tilde{s})}d\tilde{s}+\int_{-1}^{1}U_n(\tilde{s})\sqrt{1-\tilde{s}^2}\tilde{N}(\tilde{x}-\tilde{s})d\tilde{s}\right\}=-\frac{\mu\pi b}{R}\tilde{x},\quad |\tilde{x}|\leqslant 1. \tag{61}$$

It is remarked that the contact area b is not known *a priori* and will be determined from the solution of the boundary value problem. Moreover, in (61), the first integral is evaluated as a CPV integral by using the following relation (Chan et al., 2003):

$$\int_{-1}^{1}\frac{U_n(\tilde{s})\sqrt{1-\tilde{s}^2}}{(\tilde{x}-\tilde{s})}d\tilde{s}=\pi T_{n+1}(\tilde{x})\ \text{for}\ n\geqslant 0,\ |\tilde{x}|\leqslant 1. \tag{62}$$

Table 1
Flat punch. Normalized pressure $p(\tilde{x})/p_{clas}(\tilde{x})$ below the indentor at $x/b=1$ for a material with Poisson's ratio $\nu=0$.

N	$q=10$	$q=1.0$	$q=0.1$	$q=0.01$
20	1.007603	1.215746	1.654364	1.58892
40	1.007603	1.215746	1.654364	1.72365
60				1.72391
80				1.72391

Consequently, one reaches the following functional equation that can be used in the numerical discretization

$$\sum_{n=0}^{\infty} a_n \left\{ -\frac{(1-\nu)\pi}{3-2\nu} T_{n+1}(\tilde{x}) + W_n(\tilde{x}) \right\} = -\frac{\mu\pi b}{R}\tilde{x}, \tag{63}$$

where $W_n(\tilde{x}) = \int_{-1}^{1} U_n(\tilde{s})\sqrt{1-\tilde{s}^2}\tilde{N}(\tilde{x}-\tilde{s})d\tilde{s}$ is a regular integral, which can be evaluated by the standard Gauss–Chebyshev quadrature method. Now, Eq. (63) is solved by truncating the series at $n = N$ and using an appropriate collocation technique with collocation points chosen as the roots of $T_{N+1}(\tilde{x})$, viz. $\tilde{x}_j = \cos((2j-1)\pi/(2(N+1)))$ with $j = 1, 2, \ldots, N+1$. In this way, a system of $N+1$ linear algebraic equations is formed for the $N+1$ coefficients a_n. It is noted that since the index of the pertinent singular integral equation (61) is $k = -1$, the complementary condition (54) is not necessary for the computation of the system coefficients but is essential for the evaluation of the unknown contact area b. In general, in such cases where both ends of the contact area are smooth, a consistency condition should be also considered (see e.g. Gakhov, 1966). However, it can be readily shown that in our case this condition is identically satisfied. Now, for a given ratio q, all the coefficients a_n are evaluated from the solution of (63) as linear functions of the unknown contact area b. In particular, we derive a relation of the form: $a_0 = cb$, where c is a constant depending upon the values of $c \equiv c(\mu, \nu, q, P, R)$. On the other hand, utilizing the complementary condition (54) in conjunction with the representation (60) for the pressure distribution, and taking into account the orthogonality properties of the second kind Chebyshev polynomials U_n, we obtain that: $a_0 = 2P(\pi b)^{-1}$. Combining the above results regarding the coefficient a_0, a quadratic equation for b is obtained, the solution of which yields numerically the unknown contact length as: $b = (2P/\pi c)^{1/2}$.

In Table 2, the convergence of the normalized half contact width b/b_{clas} is shown.

6.3. Wedge indentor

Finally, we consider the problem of the sharp wedge indentor. As in the classical theory (Hills and Nowell, 1994), we assume that the pressure is non-singular at the end points of the contact area. In this case, the singular integral equation (53) takes the following form

$$-\frac{1-\nu}{3-2\nu}\int_{-1}^{1}\frac{p(\tilde{s})}{\tilde{x}-\tilde{s}}d\tilde{s} + \int_{-1}^{1}\tilde{N}(\tilde{x}-\tilde{s})p(\tilde{s})d\tilde{s} = -\mu\pi \operatorname{sgn}(\tilde{x})\cot\alpha, \quad |\tilde{x}| \leqslant 1, \tag{64}$$

where sgn () is the signum function, and α is the half-angle of the indentor (Fig. 1c). It is noted that the presence of the signum function on the RHS of (64) induces a discontinuity of the solution at $\tilde{x} = 0$. Therefore, the methodology employed in the previous sections, although in general converging, yet is not optimally efficient for the numerical solution of (64) and should be accordingly modified. For this reason, we follow the approach proposed by Ioakimidis (1980) for the solution of crack problems where the loading function presents jump discontinuities. An interesting application of this methodology in 2D contact problems for functionally graded materials in the context of classical elasticity can be found in Ke and Wang (2006).

Table 2
Cylindrical indentor. Normalized half contact width b/b_{clas} for a material with Poisson's ratio $\nu = 0$.

N	$q = 10$	$q = 1.0$	$q = 0.1$	$q = 0.01$
20	0.57972	0.65245	0.91512	0.99156
40	0.57972	0.65245	0.91512	0.99063
60				0.99063

To this end, we set

$$p(\tilde{x}) = \psi(\tilde{x}) + h(\tilde{x}), \tag{65}$$

where $\psi(\tilde{x})$ is a new function to be determined and $h(\tilde{x})$ satisfies the singular integral equation

$$-\frac{1-\nu}{3-2\nu}\int_{-1}^{1}\frac{h(\tilde{s})}{\tilde{x}-\tilde{s}}d\tilde{s} = -\mu\pi \operatorname{sgn}(\tilde{x})\cot\alpha, \quad |\tilde{x}| \leqslant 1. \tag{66}$$

Now, (66) has the same general form as the integral equation that describes the shallow wedge problem in the classical theory (Johnson, 1985; see also Section 7). A closed-form solution is then given by

$$h(\tilde{x}) = \frac{\mu(3-2\nu)\cot\alpha}{\pi(1-\nu)}\ln\frac{1+\sqrt{1-\tilde{x}^2}}{1-\sqrt{1-\tilde{x}^2}}. \tag{67}$$

Upon substitution from (65) into (64) and by using (66), one arrives at

$$-\frac{1-\nu}{3-2\nu}\int_{-1}^{1}\frac{\psi(\tilde{s})}{\tilde{x}-\tilde{s}}d\tilde{s} + \int_{-1}^{1}\tilde{N}(\tilde{x}-\tilde{s})\psi(\tilde{s})d\tilde{s} = f(\tilde{x}), \quad |\tilde{x}| \leqslant 1, \tag{68}$$

where

$$f(\tilde{x}) = -\int_{-1}^{1}\tilde{N}(\tilde{x}-\tilde{s})h(\tilde{s})d\tilde{s}. \tag{69}$$

Moreover, the complementary condition in (54) yields

$$\int_{-1}^{1}\psi(\tilde{x})d\tilde{x} = \frac{P}{b} - \frac{2\mu(3-2\nu)\cot\alpha}{\pi(1-\nu)}. \tag{70}$$

It can be readily shown that the function $f(\tilde{x})$ is continuous in the range $\tilde{x} \in [-1, 1]$, and thus, the standard methodology described in the previous section can be directly applied for the solution of (68). As in the cylindrical indentor case, we assume that $\psi(\tilde{s})$ has the following form

$$\psi(\tilde{s}) = \sum_{n=0}^{\infty} a_n U_n(\tilde{s})\sqrt{1-\tilde{s}^2}. \tag{71}$$

Then, omitting the details of the analysis, the final functional form of the integral equation becomes

$$\sum_{n=0}^{N} a_n \left\{ -\frac{(1-\nu)\pi}{3-2\nu} T_{n+1}(\tilde{x}) + W_n(\tilde{x}) \right\} = f(\tilde{x}). \tag{72}$$

Again, the unknown contact length b will be determined from the solution of (72) together with the complementary condition (70). The functional equation is solved by employing the same collocation scheme as in Section 6.2. In this case, the solution presented a slower convergence, when compared to the previous cases. Indeed, as it is shown in Table 3, for small values of the ratio q, a significant increase in the number of collocation points is needed for the convergence of the solution. This can be attributed to the fact that as $q \to 0$ the continuous function $f(\tilde{x})$ approaches the discontinuous signum function. In particular, taking into account (55), (66), and (69), we readily obtain that: $\lim_{q\to 0} f(\tilde{x}) = -2\mu\pi(1-\nu)\operatorname{sgn}(\tilde{x})\cot\alpha$.

7. Results and discussion

We now proceed to the discussion of the results obtained for the three indentation problems. In what follows, we investigate the effect of the ratio ℓ/b (normalized characteristic length) and the Poisson's ratio ν upon the contact pressure distribution, the contact width, and the average pressure. For the sake of completeness, we cite in Table 4 the respective solutions for the three indentation problems in the context of classical elasticity (Johnson, 1985).

Table 3
Wedge indentor. Normalized half contact width b/b_{clas} for a material with Poisson's ratio $\nu = 0$.

N	$q = 10$	$q = 1.0$	$q = 0.1$	$q = 0.01$
20	0.33614	0.43278	0.89726	0.99694
40	0.33614	0.43278	0.89532	0.99216
60			0.89519	0.99123
80			0.89517	0.99084
100			0.89516	0.99066
120			0.89516	0.99056
140				0.99046
160				0.99046

7.1. Effect of normalized characteristic length ℓ/b upon the contact pressure distributions

Fig. 2a and b depict the variation of the ratio of the couple-stress to the conventional pressure p/p_{clas} for the flat punch problem as a function of the ratio ℓ/b at various fixed normalized distances x/b. Results are shown for Poisson's ratios (a) $\nu = 0$ and (b) $\nu = 0.5$. The classical elasticity solution is represented by a single point at $\ell/b = 0$. As ℓ/b increases from zero, the results regarding the pressure below the indentor depart from those predicted by classical elasticity. In fact, it is observed that at small values of the ratio ℓ/b the couple-stress effects are more pronounced and the deviation from the classical elasticity solution is increased. The boundary layer effect near the corners of the punch is more apparent in the present representation from the curves that correspond to $x/b = 0.9$ and $x/b = 0.99$. In particular, the curve $x/b = 0.9$ reveals the effect in greater detail: following an initial steep descent below the classical pressure-ratio of unity, it rises to a maximum above unity before it steadily approaches the asymptotic value of unity common to all curves as $\ell/b \to \infty$.

Moreover, we note that the pressure below the flat punch at a fixed location and away from its corners ($|x| < 0.8b$) is always reduced compared to its classical value. This reduction is more evident in the range $0.2 < \ell/b < 0.4$. On the other hand, as $x/b \to 1$, the pressure for both classical elasticity and couple stress elasticity becomes infinite, however, since both solutions exhibit the same asymptotic behavior, their ratio remains bounded as $x/b \to 1$. In this case, as Muki and Sternberg (1965) pointed out, the pressure concentration is significantly amplified, for fixed, however small, values of ℓ in a sufficiently small neighborhood of the corners of the punch. In fact, as $x/b \to 1^-$, the pressure ratio rises abruptly from unity reaching the maximum value $\sqrt{3-2\nu}$ as $\ell/b \to 0$ and then decreases to unity as $\ell/b \to \infty$. Finally, regarding the effect of the Poisson's ratio upon p/p_{clas}, we note that for small values of ν the couple-stress effects become more significant.

Next, we proceed with the results for the cylindrical indentation problem presented in Fig. 3a and b for various normalized distances x/b. It is observed that contrary to the flat punch case, the pressure ratio p/p_{clas} is in general above unity for all values of ℓ/b. As ℓ/b increases, the material microstructure becomes more pronounced and the pressure ratio increases significantly and tends to the limit $\sqrt{3-2\nu}$. A similar behavior is noted for the shallow wedge indentation problem (Fig. 4). In this case, the effect of the ratio ℓ/b over the pressure ratio becomes more significant as we approach the sharp tip of the indentor ($x/b \to 0$) where both the classical and the couple-stress solutions exhibit logarithmic type singularities. In fact, it can be shown that as ℓ departs from zero, the strength of the pressure singularity becomes: $\lim_{x\to 0} p/p_{clas} = 3 - 2\nu$, for every ratio ℓ/b. Finally, regarding the effect of the Poisson's ratio, we note that for increasing ν the pressure ratio decreases.

Table 4
Solutions for the three indentation problems in the context of classical elasticity (Johnson, 1985).

	Flat punch	Cylindrical indentor	Wedge indentor
b	$const.$	$\sqrt{\frac{2PR(1-\nu)}{\pi\mu}}$	$\frac{P(1-\nu)}{2\mu\cot\alpha}$
$p(x)$	$\frac{P}{\pi\sqrt{b^2-x^2}}$	$\frac{2P}{\pi b^2}\sqrt{b^2-x^2}$	$\frac{\mu\cot\alpha}{(1-\nu)\pi}\ln\frac{b+\sqrt{b^2-x^2}}{b-\sqrt{b^2-x^2}}$

The distribution of the contact pressure under the flat punch is shown in Fig. 5. The pressure is now normalized with respect to the corresponding average pressure defined as $p_{av} = P/2b$. Note that the average pressure is always constant for the case of the flat punch and does not depend upon the ratio ℓ/b. Pressure distributions for $\ell/b = 0$ (classical elasticity), 0.2, 0.4, 4 and ∞ are presented. It is observed that as ℓ/b increases from zero, the curves depart from and then again approach the classical elasticity result. A marked deviation from the classical pressure distribution is found in a relative narrow band near the corners of the punch, revealing, thus, a boundary-layer effect. It is worth noting that the curves $\ell/b = 0$ (dashed line) and $\ell/b = \infty$ coincide. Finally, the effect of the Poisson's ratio ν is more important for intermediate ratios of ℓ/b, while is almost insignificant for very small or large ratios.

Accordingly, Fig. 6 presents details of the normalized pressure distribution characteristics below the cylindrical indentor. It is observed that the pressure distribution depends monotonically upon the ratio ℓ/b; note that such a response was not observed for the flat punch case. Moreover, for increasing ratios ℓ/b, the pressure below the indentor increases significantly. On the other hand, as $\ell/b \to 0$, we recover the classical elliptical pressure distribution. Finally, Fig. 7 depicts the normalized pressure distributions below the wedge indentor. As in the cylindrical indentor case, the pressure increases with increasing ratio ℓ/b and Poisson's ratio ν. As we approach the apex of the wedge indentor ($x/b \to 0$), the pressure in couple-stress elasticity becomes unbounded exhibiting a logarithmic singularity as in the classical theory.

7.2. Effect of normalized characteristic length ℓ/b upon the contact width and the average pressure

The most important information that one can obtain from indentation experiments is the contact area (that essentially reduces to a contact width in the two-dimensional case presented here) and the average pressure, which in our case are functions of the indent size ℓ/b. To this purpose, the (half) contact width b is normalized with the corresponding (half) contact width b_{clas} in classical elasticity. In the same spirit, the average pressure p_{av} is normalized with the corresponding $p_{av,clas}$. Results are shown for the three cases studied previously, i.e. the flat punch, the cylindrical and the wedge indentors.

In Fig. 8, the dependence of the normalized contact width b/b_{clas} is shown as a function of the ratio ℓ/b, for different values of the Poisson's ratio ν. In the flat punch case, the contact width is constant due to its distinct geometrical characteristics. On the other hand, the contact width for both cylindrical and wedge indentors depends strongly upon the ratio ℓ/b. It is observed that for increasing ℓ/b (or for increasing material length ℓ) the measured contact width b decreases. Interestingly, the qualitative dependence of the contact width upon ℓ/b is the same for both the cylindrical and wedge indentors. The observed response may, accordingly, be separated in three distinct regions with respect to the ratio ℓ/b. The first region extends up to $\ell/b \leqslant 0.02$, where the couple-stress effects are of minor importance to the contact width. The second region covers the range $0.02 \leqslant \ell/b \leqslant 2$, where the effect of the material microstructure upon the contact width becomes significant. Finally, for $\ell/b > 2$, a plateau is attained and no effect of the ratio ℓ/b upon the contact width or the average pressure is further observed.

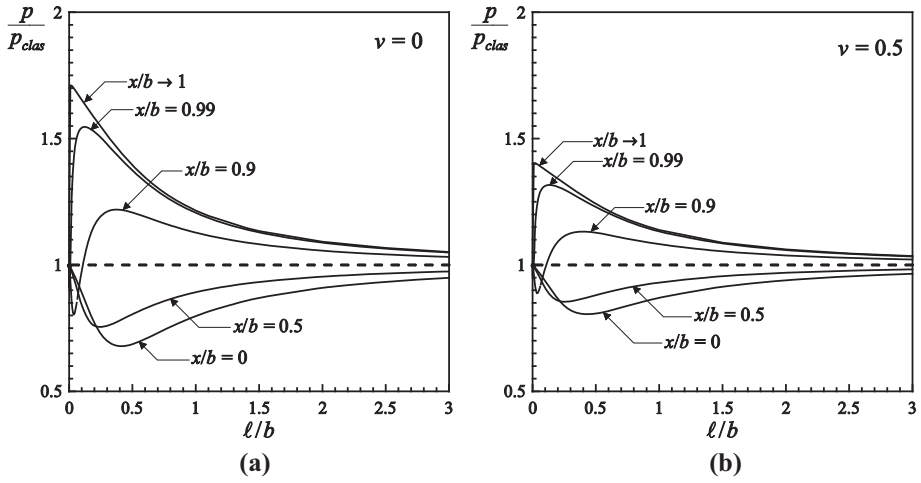

Fig. 2. Indentation of a half-plane by a rigid flat punch. Variation of the ratio of the pressure distributions in couple-stress elasticity and classical elasticity at fixed normalized distances with respect to the ratio ℓ/b. Results are shown for Poisson's ratios (a) $\nu = 0$ and (b) $\nu = 0.5$.

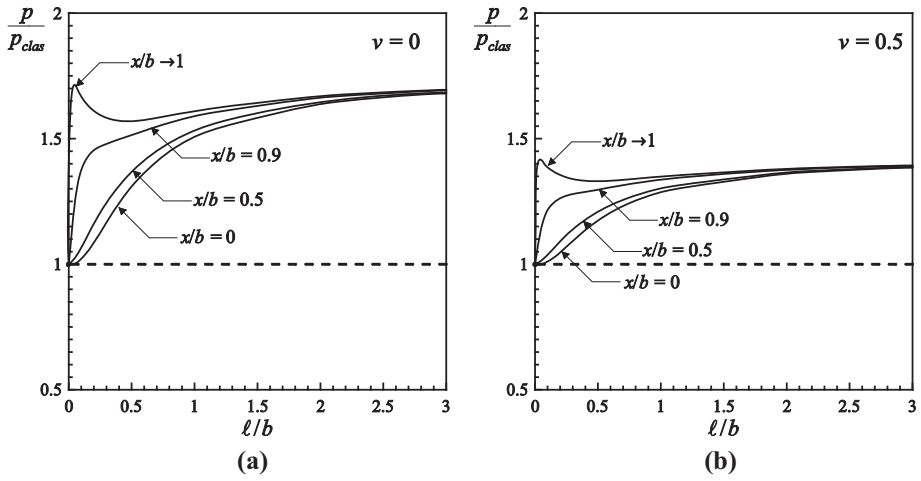

Fig. 3. Indentation of a half-plane by a rigid cylindrical indentor. Variation of the ratio of the pressure distributions in couple-stress elasticity and classical elasticity at fixed normalized distances with respect to the ratio ℓ/b. Results are shown for Poisson's ratios (a) $\nu = 0$ and (b) $\nu = 0.5$.

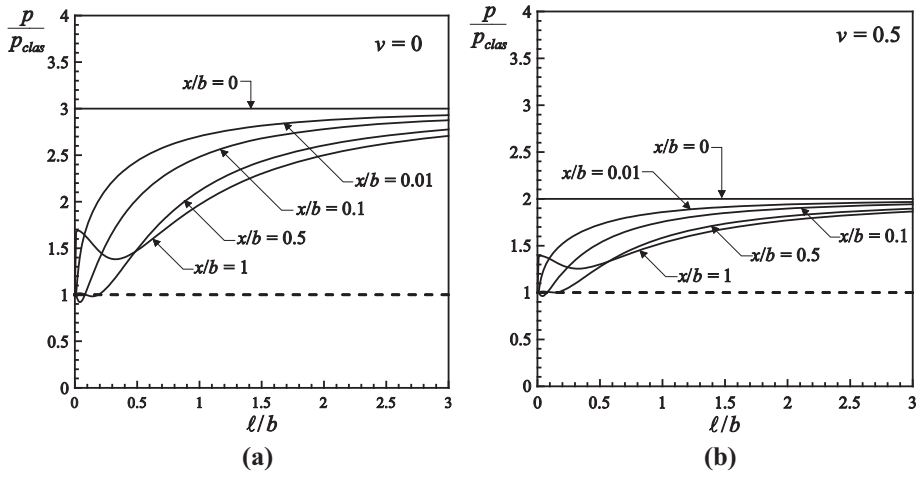

Fig. 4. Indentation of a half-plane by a rigid wedge indentor. Variation of the ratio of the pressure distributions in couple-stress elasticity and classical elasticity at fixed normalized distances with respect to the ratio ℓ/b. Results are shown for Poisson's ratios (a) $\nu = 0$ and (b) $\nu = 0.5$.

On the other hand, Fig. 9 illustrates the effect of the ratio b/ℓ on the normalized average pressure (hardness) $p_{av}/p_{av,clas}$. It is observed that when couple-stress effects are taken into account ($\ell \neq 0$), the hardness increases significantly compared to the classical prediction. For instance, in the case of a wedge indentor and for a material with $\nu = 0.3$ and $b/\ell = 2$, a 57% increase is noted in the

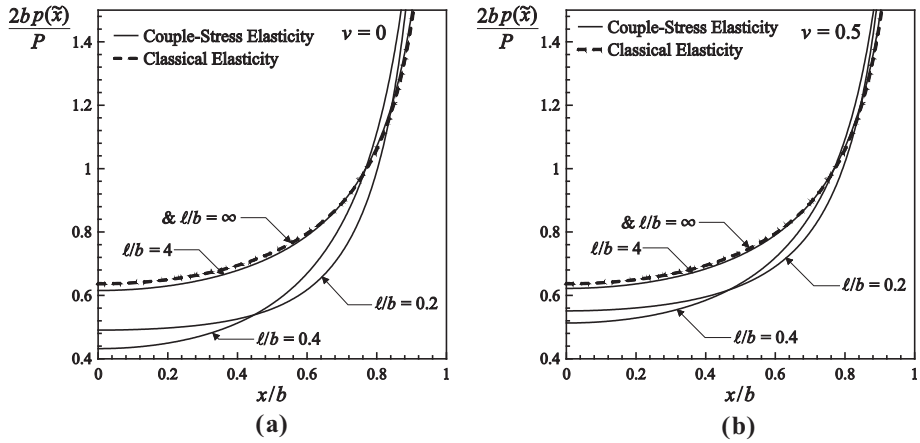

Fig. 5. Distribution of the pressure below the flat punch with respect to the normalized distance x/b for various ratios ℓ/b. Results are shown for Poisson's ratios (a) $\nu = 0$ and (b) $\nu = 0.5$.

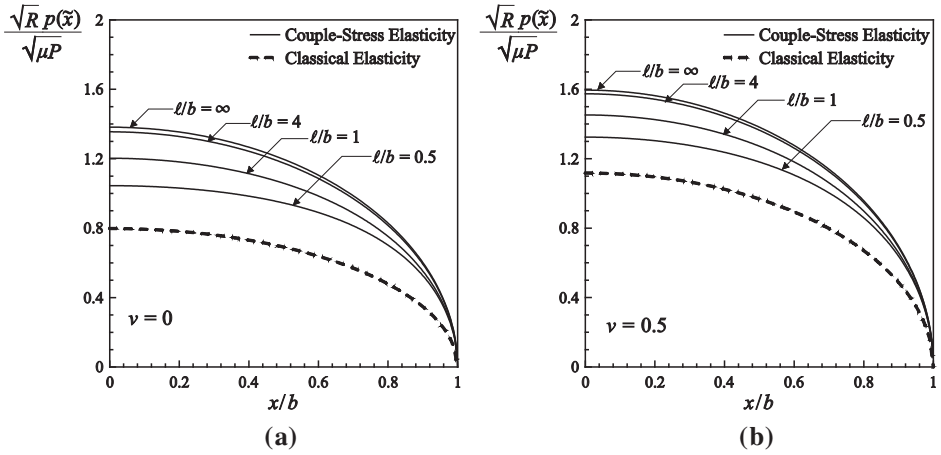

Fig. 6. Distribution of the pressure below the cylindrical indentor with respect to the normalized distance x/b for various ratios ℓ/b. Results are shown for Poisson's ratios (a) $\nu = 0$ and (b) $\nu = 0.5$.

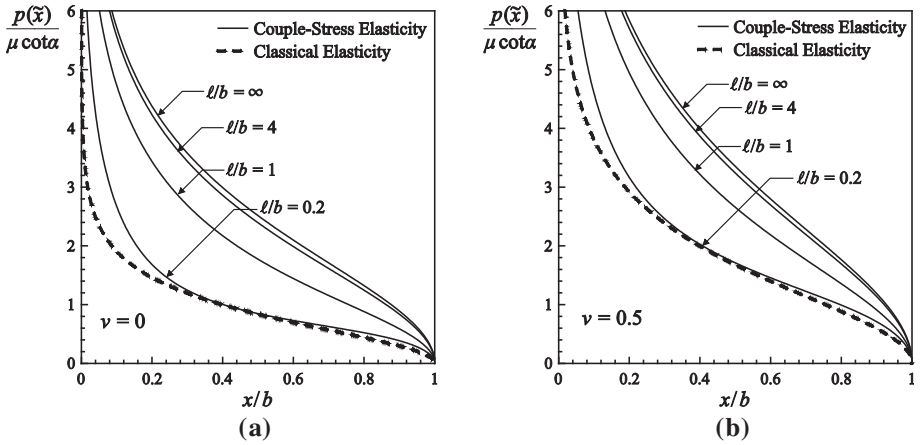

Fig. 7. Distribution of the pressure below the wedge indentor with respect to the normalized distance x/b for different ratios ℓ/b. Results are shown for Poisson's ratios (a) $\nu = 0$ and (b) $\nu = 0.5$.

average contact pressure. As b/ℓ increases the hardness decreases monotonically reaching the limit value of unity. Such indentation size effects have been reported in the experiments performed by Han and Nikolov (2007) during the *elastic* deformation of polymers and particularly of silicone. In their work they showed that the indentation size effects are strongly related to the elastic and not merely to the plastic deformation as it is reported for the size-depended deformation of metallic materials. In fact, indentation experiments with a Berkovich indentor carried out on heterochain polymers such as polycarbonate (PC), epoxy, polyethylene

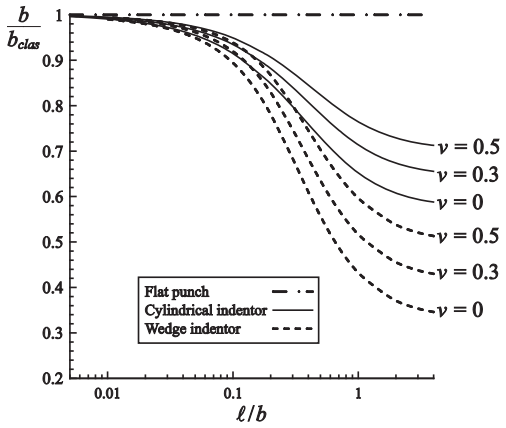

Fig. 8. Dependence of the dimensionless contact width b/b_{clas} upon the ratio ℓ/b and the Poisson's ratio ν.

terephthalate (PET) and polyamide 66 or nylon66 (PP66), showed an increased hardness with decreasing indentation depths, an experimental result which is qualitatively very similar to our p_{av} versus b relation presented in Fig. 9. Furthermore, Han and Nikolov (2007) reported that the depth at which the hardness starts to increase depends strongly, in the elastic deformation regime, upon the type of the polymer under consideration. In particular, they reported that the hardness at small indentation depths (or small contact areas) can increase from 0% to as much as 300%. In accord, our analysis showed that, depending on the Poisson ratio, a maximum increase of about 30–55% for the cylindrical and an increase of about 65–130% for the wedge indentor is attained for a contact area (lengths) twice the characteristic material length ($b/\ell = 1$) (see Fig. 9).

As a final comment, we note that despite the qualitative similarities of the wedge and the cylindrical indentors, the former is distinctively more sensitive to the ratio ℓ/b as compared to the latter. For experimental purposes, both cylindrical and wedge indentors may be used in order to extract the characteristic material length ℓ of the indented material (Figs. 8 and 9) but realistically and from a practical perspective, in the case of the wedge indentor, the use of a large wedge angle and material failure in the highly stressed region immediately below the wedge tip may limit the applicability of the present analysis. On the other hand, the cylindrical indentor, though less sensitive to the effect of length scale, is not subject to these drawbacks and may in reality be the best geometry to investigate the effect of material length scale on the behavior of a microstructured elastic material. In any case, it should be emphasized that due to the characteristic dependence of the contact width or the average pressure upon the ratio ℓ/b (or b/ℓ), in practice, experimental results regarding the internal material length may be attained in the region $0.1 < \ell/b < 1$, where this dependence is more pronounced.

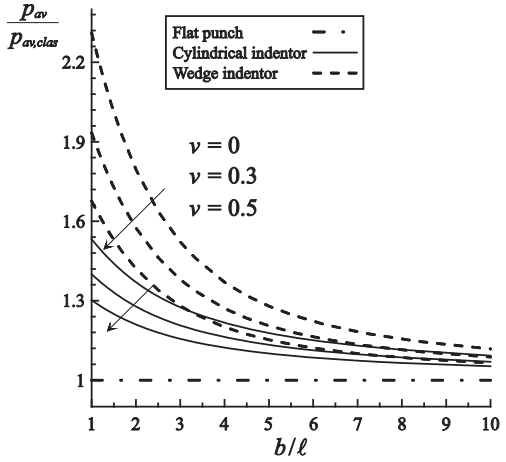

Fig. 9. Dependence of the dimensionless average pressure $p_{av}/p_{av,clas}$ upon the ratio ℓ/b and the Poisson's ratio ν.

8. Conclusions

In the present study, we derived general solutions for three basic two-dimensional plane strain contact problems within the framework of the generalized continuum theory of couple-stress elasticity. This theory introduces a characteristic material length in order to describe the pertinent scale effects that emerge from the underlying microstructure and has proved to be very effective for modeling complex microstructured materials. By using this theory, we initially studied the problem of the indentation of a deformable half-plane by a flat punch, then by a cylindrical indentor and finally by a sharp wedge indentor. Our approach is based on singular integral equations which have resulted from a treatment of the mixed boundary value problems via integral transforms and generalized functions.

The present results exhibit significant departure from the predictions of classical elasticity. In particular, for the cylindrical and wedge indentation problems, it was shown that for increasing ratio ℓ/b the pressure below the indentor increases significantly compared to the classical elasticity predictions. On the other hand, for the flat punch case the corresponding results showed that as ℓ/b increases from zero, the pressure departs from and then again approaches the classical solution. Moreover, the qualitative dependence of the contact width or the average pressure upon ℓ/b is the same for both cylindrical and wedge indentors and the general response may be separated in three distinct regions with respect to ℓ/b. It was further observed that as the characteristic material length ℓ increases the contact width b decreases. In light of the above, we conclude that it is inadequate to analyze indentation problems in microstructured complex materials employing only classical contact mechanics. In a future work, we intend to extend the present analysis to the case of three-dimensional axisymmetric indentors.

Acknowledgment

Panos A. Gourgiotis gratefully acknowledges support from the European Union FP7 project "Modeling and optimal design of ceramic structures with defects and imperfect interfaces" under contract number PIAP-GA-2011-286110.

References

Abramowitz, M., Stegun, I.A., 1972. Handbook of Mathematical Functions. Dover, New York.
Begley, M.R., Hutchinson, J.W., 1998. The mechanics of size-dependent indentation. J. Mech. Phys. Solids 46, 2049–2068.
Beveridge, A.J., Wheel, M.A., Nash, D.H., 2013. The micropolar elastic behaviour of model macroscopically heterogeneous materials. Int. J. Solids Struct. 50, 246–255.
Bigoni, D., Drugan, W.J., 2007. Analytical derivation of cosserat moduli via homogenization of heterogeneous elastic materials. ASME J. Appl. Mech. 74, 741–753.
Bower, A.F., 2009. Applied Mechanics of Solids. CRC Press, Boca Raton, FL.
Chan, Y.-S., Fannjiang, A.C., Paulino, G.H., 2003. Integral equations with hypersingular kernels theory and applications to fracture mechanics. Int. J. Eng. Sci. 41, 683–720.
Chen, J.Y., Huang, Y., Ortiz, M., 1998. Fracture analysis of cellular materials: a strain gradient model. J. Mech. Phys. Solids 46, 789–828.

Chen, X., Hutchinson, J.W., Evans, A.G., 2004. Simulation of the high temperature impression of thermal barrier coatings with columnar microstructure. Acta Mater. 52, 565–571.
Danas, K., Deshpande, V.S., Fleck, N.A., 2012. Size effects in the conical indentation of an elasto-plastic solid. J. Mech. Phys. Solids 60, 1605–1625.
Erdogan, F., 1978. Mixed boundary-value problems in mechanics. In: Nemat-Nasser, S. (Ed.), Mechanics Today. Pergamon Press, New York, pp. 1–86.
Erdogan, F., Gupta, G.D., 1972. On the numerical solution of singular integral equations. Q. Appl. Math. 29, 525–534.
Fang, W., Wickert, J.A., 1994. Post buckling of micromachined beams. J. Micromech. Microeng. 4, 116.
Fischer-Cripps, A.C., 2004. Nanoindentation. Springer, New York.
Fleck, N.A., Hutchinson, J.W., 2001. A reformulation of strain gradient plasticity. J. Mech. Phys. Solids 49, 2245–2271.
Fleck, N.A., Shu, J.Y., 1995. Microbuckle initiation in fibre composites: a finite element study. J. Mech. Phys. Solids 43, 1887–1918.
Fleck, N.A., Zisis, Th., 2010. The erosion of EB-PVD thermal barrier coatings: the competition between mechanisms. Wear 268, 1214–1224.
Fleck, N.A., Muller, G.M., Ashby, M.F., Hutchinson, J.W., 1994. Strain gradient plasticity: theory and experiment. Acta Metall. Mater. 42, 475–487.
Gakhov, F.D., 1966. Boundary Value Problems. Pergamon Press and Addison-Wesley, Oxford.
Georgiadis, H.G., Velgaki, E.G., 2003. High-frequency Rayleigh waves in materials with micro-structure and couple-stress effects. Int. J. Solids Struct. 40, 2501–2520.
Gourgiotis, P.A., Georgiadis, H.G., 2007. Distributed dislocation approach for cracks in couple-stress elasticity: shear modes. Int. J. Fract. 147, 83–102.
Gourgiotis, P.A., Georgiadis, H.G., 2008. An approach based on distributed dislocations and disclinations for crack problems in couple-stress elasticity. Int. J. Solids Struct. 45, 5521–5539.
Gourgiotis, P.A., Georgiadis, H.G., 2009. Plane-strain crack problems in microstructured solids governed by dipolar gradient elasticity. J. Mech. Phys. Solids 57, 1898–1920.
Gourgiotis, P.A., Georgiadis, H.G., 2011. The problem of sharp notch in couple-stress elasticity. Int. J. Solids Struct. 48, 2630–2641.
Grammenoudis, P., Tsakmakis, C., 2005. Finite element implementation of large deformation micropolar plasticity exhibiting isotropic and kinematic hardening effects. Int. J. Numer. Methods Eng. 62, 1691–1720.
Grentzelou, C.G., Georgiadis, H.G., 2005. Uniqueness for plane crack problems in dipolar gradient elasticity and in couple-stress elasticity. Int. J. Solids Struct. 42, 6226–6244.
Han, C.-S., Nikolov, S., 2007. Indentation size effects in polymers and related rotation gradients. J. Mater. Res. 22, 1662–1672.
Hills, D., Nowell, D., 1994. Mechanics of Fretting Fatigue. Kluwer Academic Publishers, Dordrecht.
Huang, Y., Chen, J.Y., Guo, T.F., Zhang, L., Huang, K.C., 1999. Analytic and numerical studies on mode I and mode II fracture in elastic–plastic materials with strain gradient effects. Int. J. Fract. 100, 1–27.
Huber, N., Nix, W.D., Gao, H., 2002. Identification of elastic–plastic material parameters from pyramidal indentation of thin films. Proc. R. Soc. London, Ser. A 458, 1593–1620.
Ioakimidis, N.I., 1980. The numerical solution of crack problems in plane elasticity in the case of loading discontinuities. Eng. Fract. Mech. 15, 709–716.
Johnson, K., 1985. Contact Mechanics. Cambridge University Press, Cambridge, UK.
Ke, L.-L., Wang, Y.-S., 2006. Two-dimensional contact mechanics of functionally graded materials with arbitrary spatial variations of material properties. Int. J. Solids Struct. 43, 5779–5798.
Koiter, W., 1964. Couple stresses in the theory of elasticity. Parts I and II. Nederl. Akad. Wetensch. Proc. Ser. B. 67, 17–29.
Lakes, R.S., 1983. Size effects and micromechanics of a porous solid. J. Mater. Sci. 18, 2572–2580.
Lakes, R.S., 1993. Strongly Cosserat elastic lattice and foam materials for enhanced toughness. Cell. Polym. 12, 17–30.
Lakes, R.S., Gorman, D., Bonfield, W., 1985. Holographic screening method for microelastic solids. J. Mater. Sci. 20, 2882–2888.
Larsson, P.L., Giannakopoulos, A.E., Söderlund, E., Rowcliffe, D.J., Vestergaard, R., 1996. Analysis of Berkovich indentation. Int. J. Solids Struct. 33, 221–248.
Lubarda, V.A., Markenscoff, X., 2000. Conservation integrals in couple stress elasticity. J. Mech. Phys. Solids 48, 553–564.
Ma, Q., Clarke, D.R., 1995. Size dependent hardness of silver single crystals. J. Mater. Res. 10, 853–863.
Maranganti, R., Sharma, P., 2007. A novel atomistic approach to determine strain-gradient elasticity constants: tabulation and comparison for various metals, semiconductors, silica, polymers and the (Ir) relevance for nanotechnologies. J. Mech. Phys. Solids 55, 1823–1852.
Maugin, G.A., 2010. Generalized continuum mechanics: what do we mean by that? In: Maugin, G.A., Metrikine, A.V. (Eds.), Mechanics of Generalized Continua. Springer, New York, pp. 3–13.
Mindlin, R.D., 1963. Influence of couple-stresses on stress concentrations. Exp. Mech. 3, 1–7.
Mindlin, R.D., Tiersten, H.F., 1962. Effects of couple-stresses in linear elasticity. Arch. Ration. Mech. Anal. 11, 415–448.
Muki, R., Sternberg, E., 1965. The influence of couple-stresses on singular stress concentrations in elastic solids. Z. Angew. Math. Phys. (ZAMP) 16, 611–648.
Nikolov, S., Han, C.S., Raabe, D., 2007. On the origin of size effects in smal-strain elasticity of solid polymers. Int. J. Solids 44, 1582–1592.
Nix, W.D., Gao, H., 1998. Indentation size effects in crystalline materials: a law for strain gradient plasticity. J. Mech. Phys. Solids 46, 411–425.
Paulino, G.H., Fannjiang, A.C., Chan, Y.S., 2003. Gradient elasticity theory for mode iii fracture in functionally graded materials – Part I: crack perpendicular to the material gradation. ASME J. Appl. Mech. 70, 531–542.
Pharr, G.M., Oliver, W.C., Brotzen, F.R., 1992. On the generality of the relationship among contact stiffness, contact area, and elastic modulus during indentation. J. Mater. Res. 7, 613–617.
Piccolroaz, A., Mishuris, G., Radi, E., 2012. Mode III interfacial crack in the presence of couple-stress elastic materials. Eng. Fract. Mech. 80, 60–71.
Poole, W.J., Ashby, M.F., Fleck, N.A., 1996. Micro-hardness of annealed and work-hardened copper polycrystals. Scr. Mater. 34, 559–564.
Radi, E., 2007. Effects of characteristic material lengths on mode III crack propagation in couple stress elastic–plastic materials. Int. J. Plast. 23, 1439–1456.
Reid, A.C.E., Gooding, R.G., 1992. Inclusion problem in a two-dimensional nonlocal elastic solid. Phys. Rev. B 46, 6045–6049.
Roos, B.W., 1969. Analytic Functions and Distributions in Physics and Engineering. Wiley, New York.
Shu, J.Y., Fleck, N.A., 1998. The prediction of a size effect in microindentation. Int. J. Solids Struct. 35, 1363–1383.
Stelmashenko, N.A., Walls, M.G., Brown, L.M., Milman, Y.V., 1993. Microindentations on W and Mo oriented single crystals: an STM study. Acta Metall. Mater. 41, 2855–2865.
Sternberg, E., Muki, R., 1967. The effect of couple-stresses on the stress concentration around a crack. Int. J. Solids Struct. 3, 69–95.
Stupkiewicz, S., 2007. Micromechanics of contact and interphase layers. Lecture Notes in Applied and Computational Mechanics, 30. Springer, Berlin.
Vardoulakis, I., Sulem, J., 1995. Bifurcation Analysis in Geomechanics. Blackie Academic & Professional (Chapman and Hall), London.
Wei, Y., Hutchinson, J.W., 2003. Hardness trends in micron scale indentation. J. Mech. Phys. Solids 51, 2037–2056.
Zhang, X., Sharma, P., 2005a. Inclusions and inhomogeneities in strain gradient elasticity with couple stresses and related problems. Int. J. Solids Struct. 42, 3833–3851.
Zhang, X., Sharma, P., 2005b. Size dependency of strain in arbitrary shaped anisotropic embedded quantum dots due to nonlocal dispersive effects. Phys. Rev. B 72, 195345-1–195345-16.
Zisis, Th., Fleck, N.A., 2010. The elastic–plastic indentation response of a columnar thermal barrier coating. Wear 268, 443–454.